J Mater Sci: Mater Electron (2023) 34:701

Microstructures and shear strengths of W-ball solder joints aged under isothermal and cyclic thermal conditions

Wenhui Wang[1,2], Xingke Zhao[1,2,*], Zenglei Zhao[1], and Yuhan Rong[1,2]

[1] *Shunde Innovation School, University of Science and Technology Beijing, Foshan 528399, Guangdong, China*
[2] *School of Materials Science and Engineering, University of Science and Technology Beijing, Beijing 100083, China*

Received: 16 July 2022
Accepted: 6 February 2023
Published online: 7 March 2023

ABSTRACT

The thermal reliability, which results from CTE (coefficient of thermal expansion) mismatch among packaging materials, is essential to BGA (ball grid array) packaging electronic components. For reducing the CTE mismatch, tungsten ball BGA packaging was proposed in the present study. Core–shell-structured W@Cu balls were fabricated by copper electroplating on surfaces of tungsten balls. Single-ball joint specimens were made by reflow soldering a sandwich-structured Cu/W@Cu/Cu using Sn–Ag–Cu (SAC) solder paste. Two kinds of thermal aging treatments, namely isothermal aging and cyclic thermal aging, were conducted. The microstructure and shear strength of the joints were investigated. The results show that the average shear strength of the as-soldered single-ball joint samples is 57.9 MPa. It drops to 36.8 MPa and 33.4 MPa after isothermal aged at 170 °C for 250 h and cyclic thermal aged for 500 cycles, respectively. Cu_6Sn_5 IMC layer forms at boundaries of solder/Cu and grows with either isothermal aging time or cyclic thermal aging time. The roughness of the IMC increases with cyclic thermal aging time, but it changes little during isothermal aging process. The mechanism of microstructure and property evolution of single-ball solder joints under thermal aging have been briefly discussed.

1 Introduction

BGA (ball grid array) packaging is widely used in various electronic products due to its high packing density and low cost [1, 2], which meet the needs of miniaturization, high performance, and high integration of modern electronic products [3]. However, the array-like arrangement of solder joints brings the disadvantages, such as difficult to inspection and maintenance of a defected BGA packages. Therefore, it is particularly important to increase reliability and extend service life of BGA package devices. Solder joint failure is the most common form of failure in BGA packages [4]. Unfortunately, BGA packages

Address correspondence to E-mail: xkzhao@ustb.edu.cn

https://doi.org/10.1007/s10854-023-10065-x

have greater assembly stiffness than wire bonds and are more prone to large thermal stresses inside the package. The CTE (coefficient of thermal expansion) of the constituent materials of BGA packaging systems varies widely [5, 6], result in thermal stress and fatigue damage inside the package product, especially inside the solder joints [7, 8]. The CTE mismatch of the BGA packaging material also has a stress effect on the chip, accelerating its functional degradation [9]. The thermal fatigue of solder joints caused by temperature changes during storage and service of BAG electronic components has become the main cause reducing the reliability of BGA packaged devices and shortening their service life [10]. The mechanical property analysis and fatigue life prediction of BGA solder joints have become a popular research topic in the field of electronic product reliability.

BGA balls are typically made of Sn–Ag–Cu (SAC) solders at present, since SAC solders have higher strength, good soldering performance, as well as environmental friendliness [11]. However, SAC solders have a large CTE mismatch with the chip and chip substrate and is less sustainable under harsh conditions, as compared with Sn–Pb solder [12]. Regulating the CTE mismatch of BGA packaging materials and improving their solder joint heat dissipation are fundamental ways to improve the thermal reliability of BGA packaging. Some element can improve the thermal reliability of SAC solder ball joints by refining microstructure, modifying intermetallic compounds (IMC), or improving joint metal strength [13–16]. As alloying methods change little the CTE of the SAC, it hardly reduces the thermal mismatch problem of the BGA package joints.

The CTE mismatch can be reduced by replacing SAC solder balls with Cu-cored solder balls, since the latter has a lower CTE than the former [17, 18]. In addition, Cu-cored solder balls also provide better electrical and thermal conductivity than conventional SAC solder [19, 20]. Thus, the thermal fatigues of BGA joints are improved compared with SAC solder balls [18, 21]. The CTE difference between Cu-cored ball and silicon chips or ceramic chip substrates is still large. It is necessary to fabricate solder balls using materials with a closer CTE to silicon than copper. In this study, a new kind of W-cored solder balls were prepared, and the microstructure and property evolution of tungsten-cored BGA solder joints aging at constant and alternating temperatures were investigated. By evaluating the thermal fatigue behavior of W-cored solder ball joints, the aim of this paper is to provide a reference for developing new type of BGA packaging materials and improving the reliability and service life of BGA package devices.

2 Experimental procedures

2.1 Fabrication of samples and heat treatment

The preparation process of the single solder joint sample of W-cored solder ball is shown in Fig. 1. Figure 1a, c, and e is the schematic diagrams of the devices for the preparation of tungsten balls, the preparation of tungsten solder balls, and the preparation of single-ball solder joint samples; Fig. 1b, d, and f is the photographs of the tungsten ball, tungsten solder ball, and single solder ball solder joint samples, respectively.

W balls were prepared by laser cutting commercially available W wires (diameter 0.18 mm, purity $\geq$ 99.95%) [22]. W balls with diameter of 0.3 mm were obtained by controlling the laser cutting process parameters and subsequent sieving. To improve the solderability of the W ball, a 0.1-mm-thick Cu layer was electroplated on surface of the W ball. Cu disc specimens with size of $\phi 6 \times 3$ mm were prepared by line-cutting method. A graphite layer was introduced on the surface of the Cu disks acting as a solder mask. A soldering area with $\phi 0.75$ mm in the center of graphite mask was etched by laser cleaning methods.

A single-ball joint specimen was prepared by the following two steps: (1) placing one W@Cu ball on the soldering area of one Cu disc pre-coated with SAC paste and soldering W@Cu ball to the Cu disc using reflow soldering and (2) placing another Cu disc with SAC paste pre-coated in its soldering area on the soldered W@Cu ball to form a sandwich-structured disc/ball/disc assembly and re-flowing soldering once more for the whole assembly.

The single-ball joint specimens were aging treated by either isothermal aging or cyclic thermal aging. The former was carried out at 170 °C with holding time of 30, 80, 150, and 250, respectively, and the latter was carried out with temperature alternating between 40 °C and 170 °C, the holding time at high and low temperature was 5 min and 10 min in each cycle, and cycling number was 100, 200, 300, and 500,

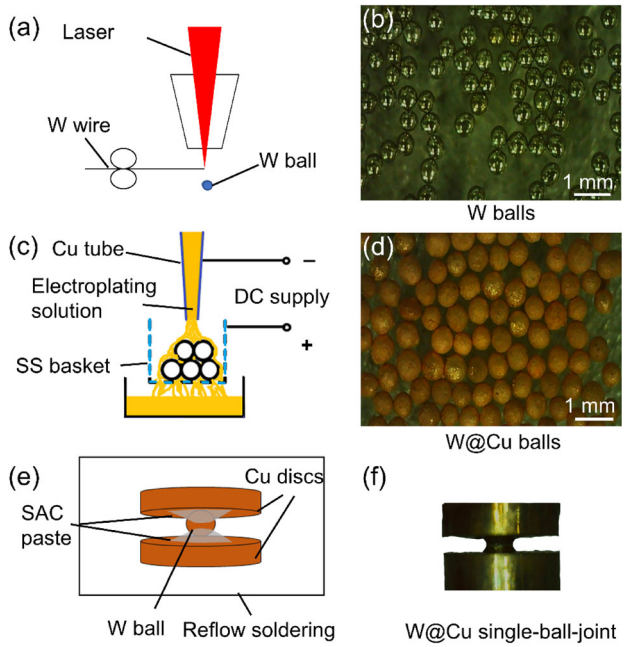

Fig. 1 Preparation illustration and samples for single tungsten ball solder joints: **a, b** for tungsten balls; **c, d** for tungsten solder balls; and **e, f** for single tungsten ball solder joints

respectively. The measured cyclic thermal aging curve is shown in Fig. 2.

2.2 Shear strength test and characterization measurement of IMC

Properties of the single-ball joint samples with or without aging treatments were determined by shear tests using a universal material testing machine (YF-900, Yangzhou Yuanfeng Testing Equipment Co., Ltd. China) and self-made jig, as shown in Fig. 3. The shear loading rate was 0.1 mm/s till the joint fractured. Three specimens were tested for each kind of joint samples and the average shear strength were calculated.

The microstructures of the single-ball joints with or without aging treatments were investigated with metallographic methods. The samples were polished and chemical etched with 4% $HNO_3 + C_2H_5OH$ solution to expose the IMC.

The thickness of the IMC layer was calculated using Eq. (1):

$$h = \frac{W_L \cdot H}{L} \times \frac{A_0}{A}, \quad (1)$$

where h is the average IMC thickness, W_L is the corresponding length of the scale in the image, H is the height of the SEM image, L is the scale length, and A_0 and A are the pixels occupied by the whole image pixel and IMC shown in the histogram, respectively.

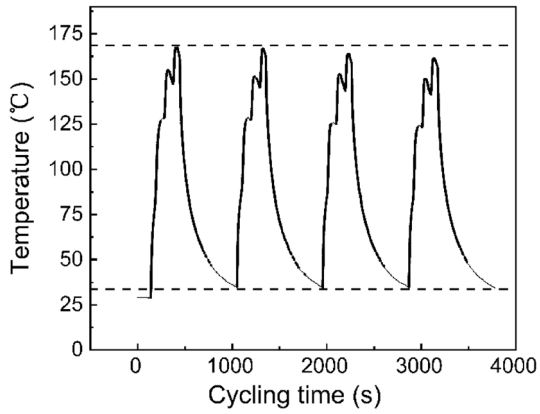

Fig. 2 40–170 °C thermal cycle temperature rise and fall curve

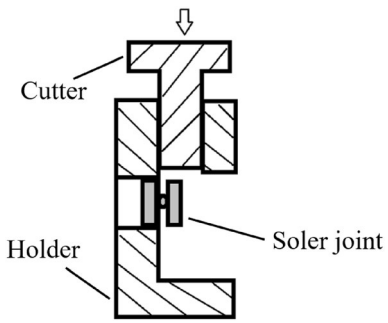

Fig. 3 Schematic diagram of sheared specimen

The morphological characteristics of the IMC layer are calculated using Eq. (2) [23]:

$$R_{rms} = \sqrt{\frac{1}{N}\sum_{i=0}^{N} y_i^2}, \quad (2)$$

where R_{rms} is the root mean square roughness, y_i is the distance between the average IMC thickness and the trough (as shown in Fig. 4), and N represents the number of data points of y_i measured. Photoshop and Origin were used to draw and combine illustrations.

3 Results

3.1 Shear strength

The average shear strength of the as-soldered single-ball joint samples was 57.9 MPa. As isothermal aging time or thermal cycling number increased, the shear strength decreased significantly. The shear strength of the sample isothermal aged at 170 °C for 250 h was

36.8 MPa, which was about 36.4% as that of the as-soldered sample. The shear strength of the sample cyclic thermal aged for 500 numbers was 33.4 MPa, which was about 42.3% as that of the as-soldered sample. The relationship between the shear strength and the thermal aging time is shown in Fig. 4, where the error bars represent standard deviation. For the cyclic thermal-aged samples, the abscissa time in Fig. 4 refers to the product of the duration of each cycle and the number of cycles and aging time, including total time. The shear strength of cyclic thermal aging-aged specimens decreased greater than that of the isothermal-aged specimens. Figure 5 gives also the fitting equations for the two curves by simulated using an exponential function.

The fitting equations are as follows:

$$\tau_1 = 31.6 + 26.8\exp(-t/155.9), \quad (3)$$

$$\tau_2 = 33.7 + 26.3\exp(-t/35.7), \quad (4)$$

where τ_1 and τ_2 in Eq. (3) and Eq. (4) are the shear strengths (MPa) of the heat aged and thermal cycling treated joints, respectively. t is aging time, which is the holding time for isothermal aging or the total time for thermal cycling aging time.

3.2 Shear fracture

By observing the macroscopic morphology of the shear fracture, it has been confirmed that there were two fracture types: solder fracture and boundary fracture, as shown in Fig. 6.

As shown in Fig. 6a 1 and a 2, the fracture paths of samples isothermal aged for 30 and 80 h were all inside the solder metal. When isothermal aging time reached 150 h, the fracture was partly inside the solder metal and partly at the solder/IMC boundary. The fractures were all at the solder/IMC boundary. Similarly, the fracture path of samples for short-time

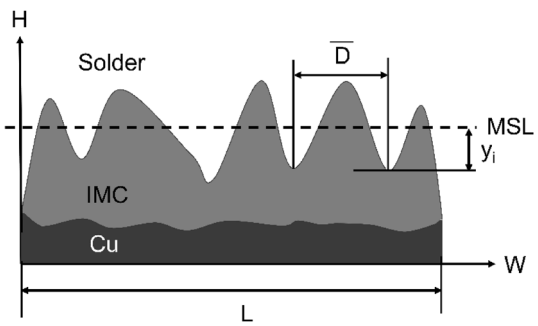

Fig. 4 Schematic diagram of IMC measurements in SEM images

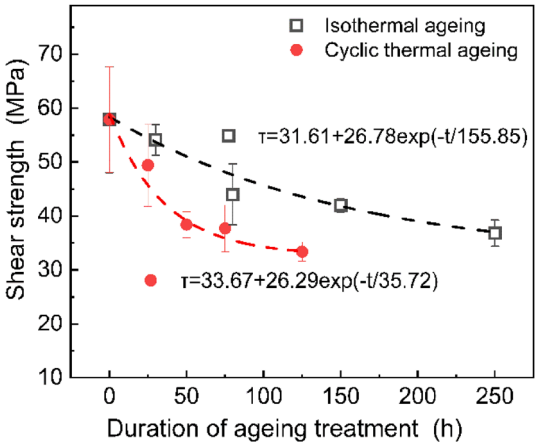

Fig. 5 Effect of thermal aging time on shear strength of the single-ball joint samples

cyclic thermal aging was inside the solder metal or at the boundary of solder/IMC, as shown in Fig. 6b1. As thermal cycle increased, the fracture a path also transferred to the boundary of solder/IMC, or partly inside the IMC layer, as shown in Fig. 6b4. In general, for isothermal-aged samples, fracture location transferred from the solder metal to the interior of the IMC as the aging time increased. For the thermal cycling-aged samples, fracture location transferred from interfacial solder to interfacial hybrid solder/IMC and to IMC as thermal cycle number increased. Therefore, all the shear fractures occur in W@Cu-ball solder joints are inside solder metal or at boundaries of solder metal and IMC layer, which is consistent with the shear behavior of common Sn-ball or Cu-cored-ball solder joints. The fracture behavior of solder joints mainly depends on characteristics of IMC layer. The present result shows that W-core has no direct effects on fracture behavior of solder joints, but exerts an indirect effect by affecting the morphology and thickness of the interfacial intermetallic compounds.

3.3 Microstructure evolution

A digitation IMC (Cu_6Sn_5) layer appeared in either the as-soldered joint or the thermal-aged joint. In the as-soldered joint, the IMC at the interface grew from the Cu substrate to the inside of the solder paste, as shown in Fig. 7.

IMC digitations in the cross-section of the thermal-aged samples are shown in Fig. 8.

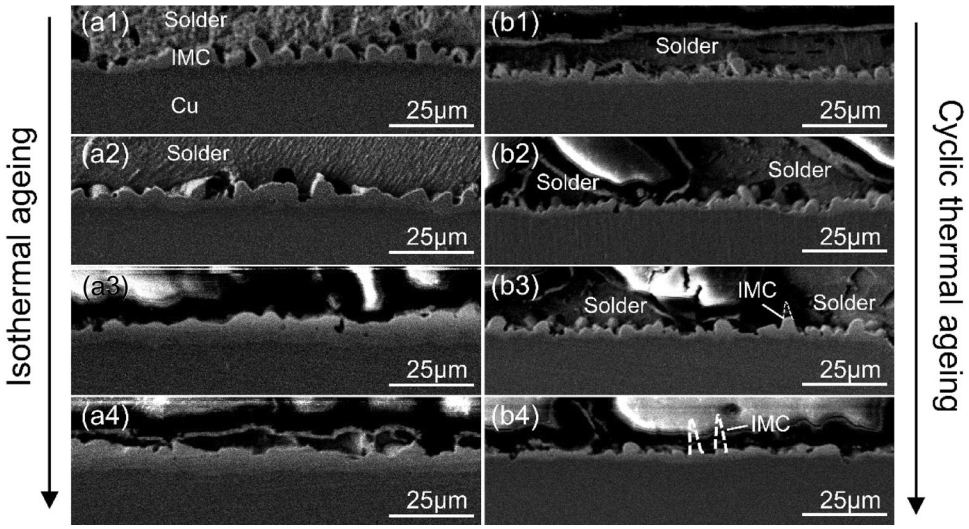

Fig.6 Shear fracture of single-ball joint samples: **a** isothermal aged at 170 °C for **a1** 30 h, **a2** 80 h, **a3** 150 h, and **a4** 250 h and **b** cyclic thermal aged between 40 °C to 170 °C for **b1** 100 cycles, **b2** 200 cycles, **b3** 300 cycles, and **b4** 500 cycles

As thermal aging time or thermal cycling number increased, the IMC digitations grew.

For the isothermal aging samples, the lateral growth rate was faster than the longitudinal growth rate, as shown in Fig. 8a1-a4; while, the opposite was true for the cyclic thermal aging temperature-aged samples, where the IMC digitations grew faster in the longitudinal direction than in the lateral direction, as shown in Fig. 8b1–b4.

Average thickness and root mean square roughness are introduced to provide a datum representation of the IMC digitations. Figure 9 is plotted with thermal aging time as the independent variable, IMC average thickness, and the root mean square roughness as the dependent variables, where the error bars are standard deviation. The broken line in Fig. 9 indicates that the average IMC thicknesses of the joints in both thermal aging methods. The IMC layer thickness of the isothermal aging samples increased in steps. At the initial stage of thermal aging ($t \leq 50$ h), the IMC layer underwent rapid growth. Afterward, the IMC growth slowed down ($50\ h < t \leq 250\ h$). When isothermal aging time exceeded 250 h, the IMC layer grew fast again. The IMC thicknesses of the as-soldered and the isothermal aged for 250 h were 2.90 μm and 9.52 μm, respectively. The IMC layer thickness of the cyclic thermal aging samples showed a continuous increasing, with no slowed down step. The IMC layer thickness of the cyclic thermal aged for 500 cycles (aging time 125 h) was 7.99 μm.

The IMC layer roughness of both thermal aging samples are plotted in the histogram in Fig. 9. For the cyclic thermal-aged samples, the roughness increased with aging time, similar as the thickness. The IMC layer roughness was about 2.06 μm for the as-soldered sample and increased to 7.65 μm. However, the IMC roughness showed no obvious difference when the as-soldered samples isothermal aged for up to 500 h. The IMC layer roughness was in range of $1.5 \sim 2.06$ μm for the isothermal-aged samples. This can also be seen from the SEM images in Fig. 8.

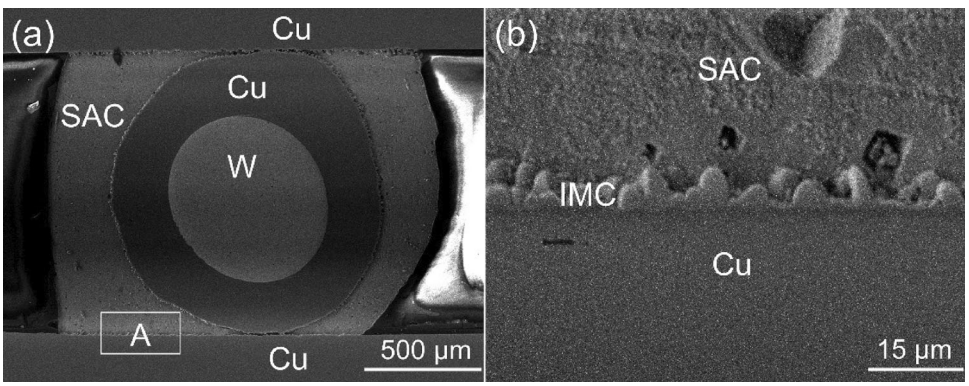

Fig. 7 Cross-sectional SEM images of the joint after reflow: **a** Diagram of the joint and **b** Partial enlargement of area A in Fig. 7a

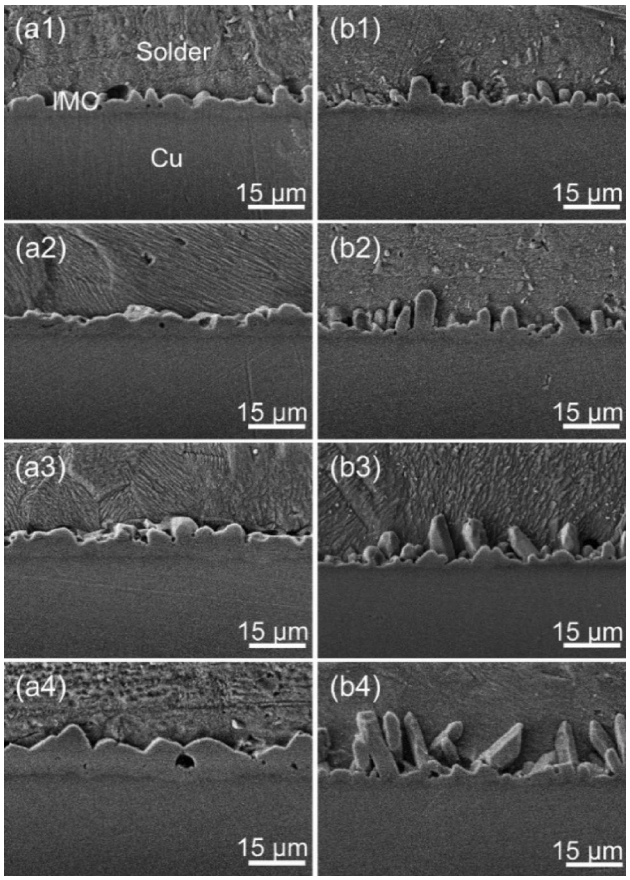

Fig. 8 IMC digitations in the cross-section of the thermal-aged samples: **a** isothermal aged at 170 °C for **a1** 30 h, **a2** 80 h, **a3** 150 h, and **a4** 250 h and **b** cyclic thermal aged between 40 °C to 170 °C for **b1** 100 cycles, **b2** 200 cycles, **b3** 300 cycles, and **b4** 500 cycles

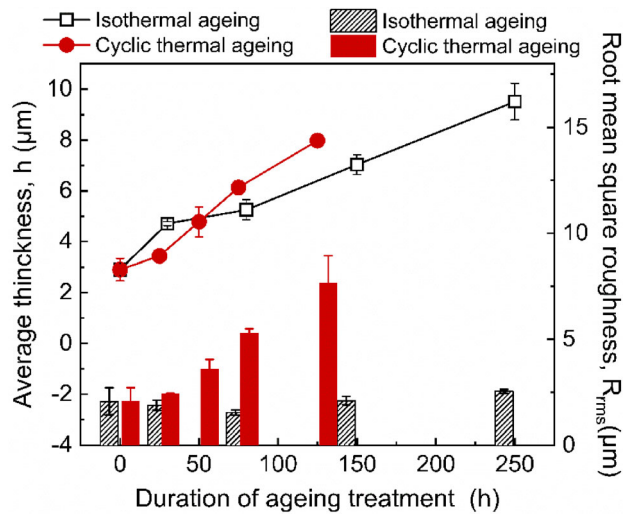

Fig. 9 Average thickness and interfacial roughness of IMC vs. heat treatment time

4 Discussion

4.1 Mechanism of IMC growth

Many studies have uncovered the formation of IMC at the interface between the lead-free solder and Cu substrate during reflow soldering. A thin Cu_6Sn_5 IMC layer is usually formed in a solid–liquid reaction system [24–26].

In the solid–solid reaction system of thermal aging, aging temperature, and aging time are the main factors controlling the final state of the IMC. Temperature controls the rate of nucleation and growth of IMC by affecting diffusion elements and diffusion mechanisms [27, 28]: from room temperature to 50–60 °C, Cu is released from the lattice as the main diffusion substance. Cu exists within Cu_6Sn_5 with a higher diffusion flux than Cu_3Sn and thus only low temperature h_0-Cu_6Sn_5 grows in this temperature range. Above 60 °C, Sn is the main diffusing material in high-temperature h-Cu_6Sn_5. At the same time, Cu_3Sn is nucleated under high-temperature drive. Cu in Cu_3Sn can diffuse in its own continuous sub-lattice; its diffusion rate is about three times that of Sn. Therefore, a certain temperature range, about 60 °C to 200 °C, Cu_3Sn grows faster, growing at the expense of Cu_6Sn_5. In other words, the low temperature limits the Cu_3Sn phase nucleation on the joint. Only at higher temperatures is it possible to generate Cu_3Sn. In addition to temperature, the limitation of too short an aging time can make Cu_3Sn grow too late [29]. The studies on the evolution of IMC during aging have been divided into two categories according to the presence or absence of Cu_3Sn phase in the IMC layer.

For the most part, Cu_6Sn_5 layer grows quickly at the initial aging stage and then the growth rate slows down with Cu_3Sn nucleating and thickening at the Cu_6Sn5/Cu interface [30–32]. A bilayer IMC structure of Sn/Cu_6Sn_5/Cu_3Sn/Cu is eventually formed in the joint. When given a sufficiently high aging temperature and long enough aging time, the joint will consist entirely of a single Cu_3Sn IMC layer [26]. However, the highest aging temperature and the longest aging time in this study are 170 °C and 250 h, respectively. The aging temperature is much larger than 60 °C, which satisfy the temperature condition that Cu_3Sn could be nucleated. The aging time is also greater than the time duration of some experiments [31] that generated double-layer IMC. Therefore, the absence of a Cu_3Sn phase in the present thermal

aging samples can only be attributed to the structure of the W ball of the joint. The growth of Cu_3Sn at the cold end in the study conducted for temperature gradient aging was inhibited by the accumulation of a large Cu flux at the interface [30]. During the reflow soldering process of solder joint formation, the copper layer on the surface of the tungsten solder ball is dissolved into the liquid tin solder, so that the content of copper in the liquid tin solder tends to reach a saturated state. When the solder joint is cooled to room temperature, the copper content of the solder joint remains high in the solder metal, reducing the copper substrate to solder metal concentration difference. During the subsequent thermal aging process, copper and tin elements diffuse in opposite directions, resulting in the growth of intermetallic compounds at the interface. The diffusion rate of copper element is higher than that of tin element, so the difference of the diffusion rate of copper and tin element determines the type and form of intermetallic compounds in the solder joint. In the tungsten solder ball joint structure of this study, the high copper content and small copper concentration gradient in the solder metal inhibit the diffusion of copper elements and hence are unfavorable to the growth of Cu_3Sn phase. Rapid growth of A on the interface layer usually results in the formation of a large number of Kirkendall cavities [29, 33]. The low number of Kirkendall voids in the IMC layer in the thermal-aged W-ball joint also proves the inhibition of Cu_3Sn growth.

4.2 IMC growth kinetics during thermal aging

The formation of IMC layer in the thermal-aged joint is related to the elements' diffusion behavior. The growth mechanism is explored by fitting the diffusion kinetic equation and calculating the activation energy and growth index [34, 35].

Prior to deriving kinetic constants of the interfacial reactions of the aged single-ball joint, some assumptions are made. (a) The Cu in the solder metal has reached saturation everywhere in the as-soldered joint. (b) Elemental diffusion and IMC growth only occur during the residence time at high temperature (i.e., 170 °C), not occur during heating, cooling, and maintaining at room temperature. (c) The growth of Cu_6Sn_5 under solid-state conditions is dominated by a time-dependent diffusion mechanism. The IMC growth can be described by following Eq. (5) and Eq. (6):

$$d - d_0 = Kt^n, \tag{5}$$

$$K = K^* \exp(-Q/RT), \tag{6}$$

where d_0 and d are the original thickness of the IMC reflow state and the thickness at the corresponding heat treatment time, respectively. t is the heat treatment time. n is the time-dependent growth index. K is the growth constant of IMC. K* is the scaling factor. Q is the activation energy of the diffusion process. R is the gas constant, and T is the absolute temperature.

Taking K* = 1.40×10^{-3} m^2/s, a power function is fitted to the heat aging time-IMC thickness, and the activation energy of K is Q = 58.65 kJ/mol, n = 0.77 for coefficient of determination (COD) = 0.96, and the growth of Cu_6Sn_5 is parabolic. A power function fit of thermal cycling time-IMC thickness is performed with COD = 0.99 at n = 1, and the growth of Cu_6Sn_5 is linear with an activation energy of Q = 68.68 kJ/mol, as shown in Fig. 10.

In fact, the value of n is taken to correspond to the dominant mechanism of IMC growth. As a rule, when n = 0.33, it corresponds to grain boundary diffusion dominance [36]; n = 0.5 for lattice diffusion dominance [35] [29]; and n = 1 for interfacial reaction-controlled growth. n = 1 mainly due to the significant increase in surface/volume ratio and the possible absence of grain boundaries in IMC. Therefore, when the size of the reaction exceeds grain size, the effect of interfacial reactions must be considered [37]. The difference in n values relative to 0.5 can also be used to represent the diffusion mechanism relative to the parabolic body diffusion control. In other studies, the fitted growth indices do not represent a specific type of diffusion. Li et al. [38] used the degree of deviation of n relative to the value of the exponent 1 representing lattice diffusion to represent the degree of deviation of the actual diffusion pattern relative to bulk diffusion, which combined with the activation energy = 19.72 kJ /mol, identified the diffusion mechanism as fan-shaped grain boundary melt channel diffusion. Where the maintenance of the diffusion channel is attributed to the selective reaction of Cu–Sn and the emission of unreacted elements.

In this study, the ideal fit is shown when n = 0.77. This indicates that the main diffusion mode in this

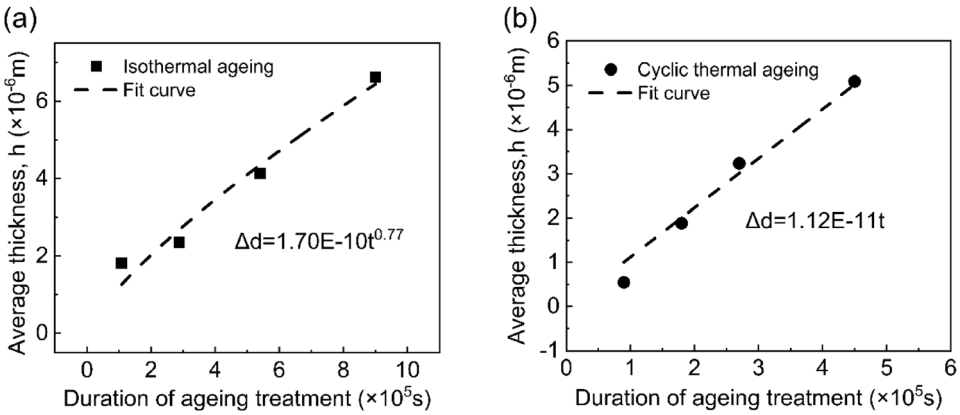

Fig. 10 The fitted relationship between IMC thickness and thermal aging time: **a** isothermal aging samples and **b** cyclic thermal aging samples

paper is between lattice diffusion and surface reaction diffusion, while the corresponding activation energy is 58.65 kJ/mol, which is closer to 64.9 kJ/mol for lattice diffusion [16]. The coupling effect of the dual interface changes the braze composition compared to the bump interface IMC where there is only one interface [34]. In addition, the increase of Cu content in the solder significantly increases the IMC growth rate. The deviation of the fit index relative to the lattice diffusion may be due to the addition of solder balls resulting in multi-interface coupling within the solder. The concentration of Cu elements in front of the boundary reaches the solid solution concentration more easily than before, the influence of surface reaction on growth increases, and in fact, the diffusion of elements within the IMC remains lattice diffusion.

4.3 Different morphologies of IMC under two thermal aging conditions

The morphology of Cu_6Sn_5 is determined by the dissolution and diffusion rates of Cu and the chemical reaction between Cu and Sn. Although the morphology of the primary Cu_6Sn_5 is not uniform owing to the uneven distribution of Cu concentration before the boundary, it is mostly scalloped and independent of adjacent crystal growth [25]. The effect of the original copper concentration in the solder on the morphology of single-phase Cu_6Sn_5 show that the lower the original Cu concentration, the lower the diffusion drive of Cu dissolution into the solder, resulting to the formation of flat structures Cu_6Sn_5 and Cu_3Sn [39, 40]. The Cu during reflow in this study is supplied not only by the substrate but also by the W ball in the solder. The dissolution of Cu occurs on both the substrate and the solder balls during the pre-reflow phase, and the time to reach the sub-stable dissolution concentration is shorter compared to the general experiments. However, since the solid–liquid reaction at the interface during the reflow occurred very quickly (a few seconds), the IMC morphology of the joints do not differ much from the IMC morphology in the previous experimental results. The formation of IMC during reflow is mainly controlled by the dissolution and reaction of Cu, which eventually form the scallop-shaped Cu_6Sn_5.

Several studies have analyzed the morphological changes during IMC growth in the solid–liquid system during reflow soldering process. The increase in heating factor may cause the transformation of Cu_6Sn_5 from corrugated to angular scallop like and the overall thickness increases [41]. In the solid–solid system during thermal aging, the scalloped Cu_6Sn_5 grows with increasing reaction time. The Cu_6Sn_5/Sn interface changes from a tilted configuration to a vertical edge crystal configuration, resulting in the interface on both sides of the IMC gradually flatting and transforming into a laminar structure [30, 33]. Physical agglomeration due to anisotropic mass flow [38], greater growth rate of scalloped IMC near the trough of the substrate [37], Gibbs free energy change [42], interface energy minimization, and interface area minimization drive associate with interface edges [33] are used to explain the IMC flattening. The patterns of IMC morphology change in most studies are summarized base on heat aging treatments, and inconsistent heat treatments often lead to different results [43]. The coupling effect of concentration gradient and diffusion anisotropy at both hot and cold ends in the case of temperature gradient (TG) aging would make the joint thickness inconsistent at

both ends and the IMC morphology much different from that under heat aging treatment conditions [30]. The grain boundary density of Cu_6Sn_5 during aging is low and growth is dominated by lattice diffusion [44]. Dynamic recrystallization of Cu_6Sn_5 during thermal cycling led to grain refinement and higher grain boundary density and the control mechanism of phase growth change to grain boundary diffusion. Thermal cycling generated stress strain inside the brazing material, changing the brazing material microstructure, and affecting the diffusion path [36]. The IMC growth is accelerated, which make the IMC, which was actually parabolic growth, show a linear relationship.

The different morphological changes and growth kinetics of IMC during the two heat treatments can be clearly observed in this study. With the increase of heat aging time, the IMC interface flattened out and the crystals gradually became uniformly planar with a parabolic kinetic curve; with the increase of thermal cycling, however, the IMC interface was more rugged and the grains grew individually with a linear kinetic curve. The IMC of the joints that undergo thermal cycling was thicker for the same duration of treatment. These phenomena are due to the anisotropic mass flow caused by different crystal orientations on the original substrate that dominates the formation of fan-shaped grains. Different thermal aging conditions can enhance or inhibit this orientation. The thermal shock effect during thermal cycling, rapid heating, and cooling generates impact thermal stresses and even micro-cracks inside the joint, and the growth of IMC toward the interior of the solder creates stresses in its tip region [16]. These two factors are coupled with each other, not only forming a fast diffusion channel in front of a single grain but also strengthening the effect of diffusion orientation inside the grain. The thermal shock also makes a large temperature difference inside and outside the joint. During the cooling process, the internal tungsten core nucleus became the hot end, dissolving a large number of Cu atoms and forming a concentration gradient. While during the heating process, the tungsten core become the cold end, creating a temperature gradient. The already nucleated IMC cannot maintain planar growth driven by the temperature and concentration gradient, and the part that was originally convex due to grain orientation enters the interior of the solder metal and its growth rate is accelerated and further convex. During a prolonged thermal cycling, a dendritic organization is formed. In contrast, the atomic diffusion inside the solder metal during thermal aging is more adequate and the concentration distribution remains relatively uniform. The projections at the interface are limited by the surface energy to continue developing and thicken in a planar shape. This is a very interesting phenomenon, and the follow-up study will focus on the growth behavior of IMC during different thermal aging treatments.

4.4 Shear strength

Shear strength of Cu/SAC305/Cu solder joints at room temperature varies considerably under different experimental conditions, with most in the range of 30 ~ 60 MPa [45–47]. Isothermal aging and cyclic thermal aging tend to reduce shear strength of solder joints [21]. A Cu-ball solder joint always has a higher shear strength than a SAC joint [20]. In addition, due to the lower CTE of Cu, the degree of plastic deformation caused by thermal cycling stresses is lower in a Cu-ball joint than in a SAC solder joint. As a result, Cu-ball solder joints also have a superior thermal cycling properties and an anti-degradation of shear strength under heat treatment conditions [18]. It should be point out that the strength results of thermal-aged solder joint in the present work show no advantages over conventional Cu-cored solder joints. The reason is not difficult to understand. In this study, two copper substrates were used to make solder joints, and the thermal mismatch between tungsten solder balls and copper substrates was higher than that of copper solder balls and copper substrate. The structure of this solder joint sample is different from that of the BGA package, which has a silicon chip and a ceramic substrate on both sides of the solder ball. The thermal mismatch between tungsten and silicon chips/ceramic substrates is smaller than that of copper and chips/ceramic substrates. Therefore, it can be expected that the solder joint samples made of silicon chips and ceramic substrates and tungsten solder balls will be better than copper solder balls. Solder joint samples. In addition, the tungsten core can coordinate the deformation of silicon and Cu substrate during the heat treatment process, which is expected to solidify further the connection strength in the primary package structure.

The changes in the microstructure of W-ball joints undergoing thermal aging have many similarities to those of copper-cored joints. The addition of copper layer increases the accumulation of Cu and inhibits the nucleation and growth of Cu_3Sn on the interfacial layer. The formation of Cu_3Sn is detrimental to the mechanical properties of the joint. Once the stress exists inside the joint, the different degree of deformation of the double-layer IMC will lead to microscopic cracking. In addition, the rapid diffusion of Cu during Cu_3Sn growth tends to form lamellar or dispersed Kirkendall voids at the Cu_6Sn_5/Cu interface. The increase in size of the Kirkendall voids after mutual engulfment not only deteriorates the electrical and thermal conductivity of the joint but also tends to become a source of internal cracks, causing the joint to fracture within the Cu_3Sn [35]. Therefore, the addition of tungsten-cored weld balls is beneficial for the joint strength from the microstructural point of view.

Microstructures have vital influence on shear strength of solder joints. The discussion on the microstructural changes inside the joint during aging is divided into two main aspects: solder and IMC. The microstructure of the solder coarsens with increasing thermal aging time [36]. IMC growth on the joint and coarsening of the internal microstructure leads to softening of the solder and a significant decrease in the reliability of the joint [48]. Moreover, during cyclic thermal aging, the IMC, substrate, and solder at the interface undergo expansion and contraction with temperature changes due to different CTE. The accumulation of thermal stress inside the solder is much greater than the stress from IMC growth on the interface during heat aging. One of the major reasons why the shear strength of cyclic thermal-aged joints decreases more rapidly.

The thickness and morphology of the IMC layer are also important factors affecting the shear strength of the two kinds of thermal-aged joints in this study. Figure 11 shows the relationship between shear strength and IMC layer of the thermal-aged samples. It is clear that the degrading of the shear strength for the cyclic aged samples ascribes to the simultaneous increase in both thickness and roughness of the IMC layers, as shown in Fig. 11a. While for the isothermal-aged samples, the degradation of the shear strength is mainly determined by the IMC thickness, as shown in Fig. 11b.

The increase in IMC thickness makes the brittle IMC a fast path for crack expansion, causing a reduction in solder joint strength. At the same IMC thickness, the long-term non-uniform growth of IMC on the cyclic thermal-aged joint leads to the accumulation of longitudinal deformation stresses. The stress concentration at prominent Cu_6Sn_5 grain root is severe, further weakening the solder joint [23], and the specimen exhibits grain penetration fracture after multiple cycle heat treatments. In addition, the cyclic thermal-aged IMC layer contains more dislocations and cracks, making the joint more susceptible to damage. In contrast, the flat IMC interface of isothermal-aged joints can improve the bond strength of IMC due to the less stress accumulation [37].

It is worth mentioning that the results reported in the present study are the author's preliminary works in attempting to use tungsten core solder balls to reduce the CTE mismatch in BGA packaging. Thus, the simplest and cheapest copper/solder ball/copper structure sample of the structure is selected to start this research work to evaluate preliminarily the technical feasibility of this tungsten solder ball for BGA. The preliminary findings obtained in this study show that it is feasible to fabricate W@Cu solder ball solder joints. In future, the chip/tungsten ball/ceramic substrate solder joint samples will be prepared and their thermal stability will be studied systematically.

5 Conclusion

In this study, Core–shell-structured W@Cu balls were prepared by laser cutting and electric-plating process, and single-ball solder joints were prepared by reflow soldering process. The microstructure and shear strength of solder joints of isothermal aging or cyclic thermal aging were investigated.

(1) The average shear strength of as-soldered single-ball joint samples was 57.9 MPa. It dropped to 36.8 MPa and 33.4 MPa after isothermal aged at 170 °C for 250 h and cyclic thermal aged for 500 cycles, respectively.

(2) Thicknesses of Cu_6Sn_5 IMC layer formed at boundaries of solder/Cu and grew thick with either isothermal aging time or cyclic thermal aging time. The roughness of the IMC layer increased with cyclic thermal aging time, but changed little with isothermal aging time.

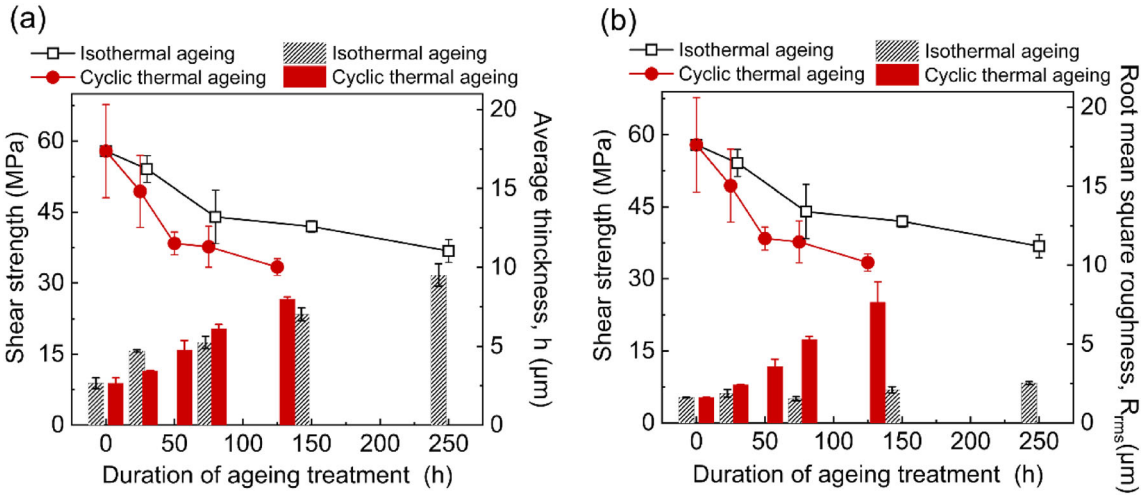

Fig. 11 Shear strength of joints vs. microstructures: an average thickness vs. shear strength and b root mean square roughness vs. shear strength

(3) Only single-IMC phase layer of Cu_6Sn_5 appeared in all the joints in the present work. The main factor controlling IMC layer growth considered to lattice diffusion according to the fitting results of IMC thickness.

Acknowledgements

This work was financially supported by the Key-Area Research and Development Program of Guangdong Province, China (No. 2019B90907002) and the Scientific and Technological Innovation Foundation of Foshan Government, (No. BK21BE003).

Author contributions

All authors contributed to the study conception and design. Material preparation, data collection, and analysis were performed by WW, XZ, ZZ, and YR. WW wrote the first draft of the manuscript, and all authors commented on previous versions of the manuscript. All authors read and approved the final manuscript.

Funding

This work was financially supported by the Key-Area Research and Development Program of Guangdong Province, China (No. 2019B90907002) and the Scientific and Technological Innovation Foundation of Foshan Government, (No. BK21BE003). Author [Xingke Zhao] has received the above research supports.

Data availability

All data generated or analyzed during this study are included in this published article.

Declarations

Conflict of interests The authors declare that they have no conflict of interest.

References

1. J. Huang, M. Zhou, S. Liang, X. Zhang, Size effects on the interfacial reaction and microstructural evolution of Sn-ball/Sn30Ag05Cu-paste/Cu joints in board-level hybrid BGA interconnection at critical reflowing temperature. J. Mater. Sci. **29**(9), 7651–7660 (2018). https://doi.org/10.1007/s10854-018-8758-0
2. I. Shohji, H. Mori, Y. Orii, Solder joint reliability evaluation of chip scale package using a modified Coffin-Manson equation. Microelectron. Reliab. **44**(2), 269–274 (2004). https://doi.org/10.1016/j.microrel.2003.08.015
3. J. Ren, M.L. Huang, Board-level drop reliability and fracture behavior of low-temperature soldering Sn–Ag–Cu/Sn–Bi–X hybrid BGA solder joints for consumer electronics. J. Mater.

Sci. **32**(11), 15453–15465 (2021). https://doi.org/10.1007/s10854-021-06094-z

4. A. Bandaram, Reliability of solder attachment options with lead free for 0.4 mm micro BGA packages. http://hdl.handle.net/10415/2626
5. P. Borgesen, L. Wentlent, S. Hamasha, S. Khasawneh, S. Shirazi, D. Schmitz, T. Alghoul, C. Greene, L. Yin, A mechanistic thermal fatigue model for SnAgCu solder joints. J. Electron. Mater. **47**(5), 2526–2544 (2018). https://doi.org/10.1007/s11664-018-6121-0
6. S. Hamasha, P. Borgesen, Effects of strain rate and amplitude variations on solder joint fatigue life in isothermal cycling. J. Electron. Packag. **138**(2), 1–9 (2016). https://doi.org/10.1115/1.4032881
7. R. Satoh, K. Arakawa, M. Harada, K. Matsui, Thermal fatigue life of Pb-Sn alloy interconnections. IEEE Trans. Compd. Hybrids, Manuf. Technol. **14**(1), 224–232 (1991). https://doi.org/10.1109/33.76537
8. Y. Chen, J. Jia, H. Fu, Z. Zeng, Analysis of the BGA solder Sn–3.0Ag–0.5Cu crack interface and a prediction of the fatigue life under tensile stress. Int. J. Fatigue **87**, 216–224 (2016). https://doi.org/10.1016/j.ijfatigue.2016.02.003
9. K. Morooka, Y. Kariya, Thermal fatigue life prediction of BGA solder joints using a creep constitutive equation incorporating microstructural coarsening effect. Mater. Trans. **62**(2), 205–212 (2021). https://doi.org/10.2320/matertrans.MT-M2020313
10. E. Suhir, R. Ghaffarian, J. Nicolics, Could thermal stresses in a BGA/CGA-system be evaluated from a model intended for a homogeneously bonded assembly. J. Mater. Sci. **27**(1), 570–579 (2015). https://doi.org/10.1007/s10854-015-3790-9
11. T. You, Y. Kim, W. Jung, J. Moon, H. Choe, Effect of surface finish on the fracture behavior of Sn–Ag–Cu solder joints during high-strain rate loading. J. Alloys Compd. **486**(1–2), 242–245 (2009). https://doi.org/10.1016/j.jallcom.2009.07.085
12. Q. Yan et al., Thermal fatigue of SnPb and SAC resistor joints: analysis of stress-strain as a function of cycle parameters. IEEE Trans. Adv. Packag. **29**(4), 690–700 (2006). https://doi.org/10.1109/tadvp.2006.884805
13. L. Gao et al., Effect of alloying elements on properties and microstructures of SnAgCu solders. Microelectron. Eng. **87**(11), 2025–2034 (2010). https://doi.org/10.1016/j.mee.2010.04.007
14. Y. Zhong et al., The influence of strengthening and recrystallization to the cracking behavior of Ni, Sb, Bi alloyed SnAgCu solder during thermal cycling. Mater. Sci. Eng. A **652**, 264–270 (2016). https://doi.org/10.1016/j.msea.2015.10.072
15. J. Xian, G. Zeng, S.A. Belyakov, Q. Gu, K. Nogita, C.M. Gourlay, Anisotropic thermal expansion of Ni3Sn4, Ag3Sn, Cu3Sn, Cu6Sn5 and βSn. Intermetallics **91**, 50–64 (2017). https://doi.org/10.1016/j.intermet.2017.08.002
16. T.K. Zhu et al., Improving tensile strength of SnAgCu/Cu solder joint through multi-elements alloying. Mater. Today Commun. (2021). https://doi.org/10.1016/j.mtcomm.2021.102768
17. S. Ikuo, S. Yuji, Y. Hiroshi, Growth Kinetics of reaction layers in flip chip joints with Cu-cored lead-free solder balls. Mater. Trans. **45**(3), 754–758 (2004). https://doi.org/10.2320/matertrans.45.754
18. Y. Kim, H. Choi, H. Lee, D. Shin, J. Cho, H. Choe, Improved reliability of copper-cored solder joints under a harsh thermal cycling condition. Microelectron. Reliab. **52**(7), 1441–1444 (2012). https://doi.org/10.1016/j.microrel.2012.03.001
19. Y. Kim, H. Choi, H. Lee, D. Shin, J. Moon, H. Choe, Fracture behavior of Cu-cored solder joints. J. Mater. Sci. **46**(21), 6897–6903 (2011). https://doi.org/10.1007/s10853-011-5654-x
20. H. Jeong, C.J. Lee, K.D. Min, J.Y. Son, S.B. Jung, Mechanical properties of Cu-core solder balls with ENEPIG surface finish. J. Electron. Mater. **49**(10), 6073–6079 (2020). https://doi.org/10.1007/s11664-020-08338-w
21. C. Chen, H. Lin, Interfacial reactions and mechanical properties of ball-grid-array solder joints using Cu-cored solder balls. J. Electron. Mater. **35**(11), 1937–1946 (2006). https://doi.org/10.1007/s11664-006-0297-4
22. S. Wang, X. Zhao, Z. Zhao, P. W, Spherical molybdenum powders prepared by pulse laser wire cutting. Powder Metall. Technol. **40**(3), 232–238 (2022). https://doi.org/10.19591/j.cnki.cn11-1974/tf.2021050009
23. T. An, F. Qin, Effects of the intermetallic compound microstructure on the tensile behavior of Sn3.0Ag0.5Cu/Cu solder joint under various strain rates. Microelectron. Reliab. **54**(5), 932–938 (2014). https://doi.org/10.1016/j.microrel.2014.01.008
24. S.U. Mehreen, K. Nogita, S.D. McDonald, H. Yasuda, D.H. StJohn, Peritectic phase formation kinetics of directionally solidifying Sn-Cu alloys within a broad growth rate regime. Acta Mater. **220**, 117295 (2021). https://doi.org/10.1016/j.actamat.2021.117295
25. T. Laurila, V. Vuorinen, J.K. Kivilahti, Interfacial reactions between lead-free solders and common base materials. Mater. Sci. Eng. R **49**(1–2), 1–60 (2005). https://doi.org/10.1016/j.mser.2005.03.001
26. S. Wang, L. Hsu, N. Wang, C. Ho, EBSD investigation of Cu-Sn IMC microstructural evolution in Cu/Sn-Ag/Cu microbumps during isothermal annealing. J. Electron. Mater. **43**(1), 219–228 (2013). https://doi.org/10.1007/s11664-013-2675-z

27. H.C. Bhedwar, K.K. Ray, S.D. Kulkarni, Kirkendall effect studies in copper-tin difpusion couples. Scr. Metall. **6**, 919–922 (1972). https://doi.org/10.1016/0036-9748(72)90145-7
28. K.N. Tu, R.D. Thoimpson, Kinetics of interfacial reaction in bimetallic Cu-Sn thin films. Acta Metall. **30**, 947–952 (1982). https://doi.org/10.1016/0001-6160(82)90201-2
29. Y. Liu, Y. Chu, K.N. Tu, Scaling effect of interfacial reaction on intermetallic compound formation in Sn/Cu pillar down to 1 μm diameter. Acta Mater. **117**, 146–152 (2016). https://doi.org/10.1016/j.actamat.2016.07.004
30. Y. Qiao, H. Ma, F. Yu, N. Zhao, Quasi-in-situ observation on diffusion anisotropy dominated asymmetrical growth of Cu-Sn IMCs under temperature gradient. Acta Mater. **217**, 17168 (2021). https://doi.org/10.1016/j.actamat.2021.117168
31. Y. Kong, Z. Kong, F. Shi, Microstructure and mechanical property of Sn–Ag–Cu solder material. Rare Met. **36**(3), 193–197 (2015). https://doi.org/10.1007/s12598-015-0579-1
32. Y. Yang, Y. Li, H. Lu, C. Yu, J. Chen, Interdiffusion at the interface between Sn-based solders and Cu substrate. Microelectron. Reliab. **53**(2), 327–333 (2013). https://doi.org/10.1016/j.microrel.2012.08.013
33. Q. Yin, F. Gao, Z. Gu, J. Wang, E.A. Stach, G. Zhou, Interface dynamics in one-dimensional nanoscale Cu/Sn couples. Acta Mater. **125**, 136–144 (2017). https://doi.org/10.1016/j.actamat.2016.11.051
34. X. Li, M. Zhou, J. Xia, M. Xiao, X. Zhang, Effect of the cross-interaction on the formation and evolution of intermetallic compounds in Cu(Ni)/Sn-Ag-Cu(Ni) BGA structure solder joints. Acta Metall. Sin. **47**(05), 611–619 (2011). https://doi.org/10.3724/SP.J.1037.2011.00063
35. X. Hu, T. Xu, L.M. Keer, Y. Li, X. Jiang, Microstructure evolution and shear fracture behavior of aged Sn3Ag0.5Cu/Cu solder joints. Mater. Sci. Eng. A **673**, 167–177 (2016). https://doi.org/10.1016/j.msea.2016.07.071
36. Q. Li, C. Li, W. Zhang, W. Chen, Z. Liu, Microstructural evolution and failure mechanism of 62Sn36Pb2Ag/Cu solder joint during thermal cycling. Microelectron. Reliab. **99**, 12–18 (2019). https://doi.org/10.1016/j.microrel.2019.05.015
37. M.M. Dhobe, I.K. Chopde, C.L. Gogte, Optimization of wire electro discharge machining parameters for improving surface finish of cryo-treated tool steel using DOE. Mater. Manuf. Processes **29**(11–12), 1381–1386 (2014). https://doi.org/10.1080/10426914.2014.930890
38. J.F. Li, A.P. Agyakwa, C.M. Johnson, Interfacial reaction in Cu/Sn/Cu system during the transient liquid phase soldering process. Acta Mater. **59**(3), 1198–1211 (2011). https://doi.org/10.1016/j.actamat.2010.10.053
39. K.P. Somashekhar, N. Ramachandran, J. Mathew, Modeling and Optimization of Process parameters in micro wire EDM by genetic algorithm. Adv. Mater. Res **76–78**, 566–570 (2009). https://doi.org/10.4028/www.scientific.net/AMR.76-78.566
40. R. Srikanth, B. Singaravel, P. Vinod, S. Aravind, D. Subodh, Optimization of process parameters in Electric Discharge Machining Process of Ti-6Al-4V alloy using hybrid Taguchi based MOORA method. IOP Conf. Ser.: Mater. Sci. Eng. **1057**(1), 012064 (2021). https://doi.org/10.1088/1757-899X/1057/1/012064
41. D. Hu, J. Shen, X. Chen, D.J. Zhai, R.H. Gao, Fracture mechanism of Sn-Cu intermetallic compound layer in BGA solder joint induced by sinusoidal vibration. Chinese J. Nonfer. Metals **29**(04), 756–763 (2019). https://doi.org/10.19476/j.ysxb.1004.0609.2019.04.12
42. B.S.S. Chandra, J. Weng, L. Shen, T.K. Lee, K.Y. Zeng, Morphology and mechanical properties of intermetallic compounds in SnAgCu solder joints. Microelectron. Eng. **87**(11), 2416–2422 (2010). https://doi.org/10.1016/j.mee.2010.04.017
43. J. Chen, Y. Yin, J. Ye, Y. Wu, Investigation on fatigue behavior of single SnAgCu/SnPb solder joint by rapid thermal cycling. Soldering Surf. Mount Technol. **27**(2), 76–83 (2015). https://doi.org/10.1108/ssmt-05-2014-0010
44. A.R. Fix, W. Nüchter, J. Wilde, Microstructural changes of lead-free solder joints during long-term ageing, thermal cycling and vibration fatigue. Soldering Surf. Mount Technol. **20**(1), 13–21 (2008). https://doi.org/10.1108/09540910810861440
45. W. Li, J. Gui, H. Qin, D. Prof, D. Yang, Shear performance of microscale ball grid array structure Cu(Ni)/Sn–30Ag–05Cu/Cu(Ni) solder joints at low temperatures. Mater. Today Commun. (2022). https://doi.org/10.1016/j.mtcomm.2022.103149
46. Y. Wang et al., Shear performance of microscale BGA structure Cu/Sn-3.0Ag-0.5Cu/Cu joints with shrinking volume at low and cryogenic temperatures ©2020 IEEE. 1–4, (2019).
47. H.B. Qin, X.P. Zhang, M.B. Zhou, X.P. Li, Y.W. Mai, Geometry effect on mechanical performance and fracture behavior of micro-scale ball grid array structure Cu/Sn–3.0Ag–0.5Cu/Cu solder joints. Microelectron. Reliab. **55**(8), 1214–1225 (2015). https://doi.org/10.1016/j.microrel.2015.05.013
48. J. Gong, C. Liu, P.P. Conway, V.V. Silberschmidt, Modelling of Ag_3Sn coarsening and its effect on creep of Sn–Ag eutectics. Mater. Sci. Eng., A. (2006). https://doi.org/10.1016/j.msea.2006.04.034